Journal of the National Cancer Center 4 (2024) 263–279

Contents lists available at ScienceDirect

Journal of the National Cancer Center

journal homepage: www.elsevier.com/locate/jncc

Full Length Article

DCS, a novel classifier system based on disulfidptosis reveals tumor microenvironment heterogeneity and guides frontline therapy for clear cell renal carcinoma

Aimin Jiang[1,†], Wenqiang Liu[1,†], Ying Liu[1,†], Junyi Hu[2,†], Baohua Zhu[1,†], Yu Fang[1], Xuenan Zhao[3], Le Qu[4], Juan Lu[5], Bing Liu[6], Lin Qi[7,8,*], Chen Cai[9,*], Peng Luo[10,*], Linhui Wang[1,*]

[1] Department of Urology, Changhai Hospital, Naval Medical University (Second Military Medical University), Shanghai, China
[2] Department of Urology, Tongji Hospital, Tongji Medical College, Huazhong University of Science and Technology, Wuhan, China
[3] Center for Translational Medicine, Naval Medical University (Second Military Medical University), Shanghai, China
[4] Department of Urology, Affiliated Jinling Hospital, Medical School of Nanjing University, Nanjing, China
[5] Vocational Education Center, Naval Medical University (Second Military Medical University), Shanghai, China
[6] Department of Urology, The Third Affiliated Hospital, Naval Medical University (Second Military Medical University), Shanghai, China
[7] Department of Orthopedics, The Second Xiangya Hospital, Central South University, Changsha, China
[8] Hunan Key Laboratory of Tumor Models and Individualized Medicine, The Second Xiangya Hospital, Changsha, China
[9] Department of Special Clinic, Changhai Hospital, Naval Medical University (Second Military Medical University), Shanghai, China
[10] Department of Oncology, Zhujiang Hospital, Southern Medical University, Guangzhou, China

ARTICLE INFO

Keywords:
Pancancer
Disulfidptosis
Multi omics
Tumor microenvironment
Tumor related pathways

ABSTRACT

Background: Emerging evidence suggests that cell deaths are involved in tumorigenesis and progression, which may be treated as a novel direction of cancers. Recently, a novel type of programmed cell death, disulfidptosis, was discovered. However, the detailed biological and clinical impact of disulfidptosis and related regulators remains largely unknown.

Methods: In this work, we first enrolled pancancer datasets and performed multi-omics analysis, including gene expression, DNA methylation, copy number variation and single nucleic variation profiles. Then we deciphered the biological implication of disulfidptosis in clear cell renal cell carcinoma (ccRCC) by machine learning. Finally, a novel agent targeting at disulfidptosis in ccRCC was identified and verified.

Results: We found that disulfidptosis regulators were dysregulated among cancers, which could be explained by aberrant DNA methylation and genomic mutation events. Disulfidptosis scores were depressed among cancers and negatively correlated with epithelial mesenchymal transition. Disulfidptosis regulators could satisfactorily stratify risk subgroups in ccRCC, and a novel subtype, DCS3, owning with disulfidptosis depression, insensitivity to immune therapy and aberrant genome instability were identified and verified. Moreover, treating DCS3 with NU1025 could significantly inhibit ccRCC malignancy.

Conclusion: This work provided a better understanding of disulfidptosis in cancers and new insights into individual management based on disulfidptosis.

1. Introduction

Renal cell cancer (RCC) remains the most malignant disease of the urological system and is one of the top 10 most common cancers in the world.[1,2] The latest global cancer statistics show a 6.6% increase in new cases and a 4.2% increase in deaths worldwide in 2023 when compared with data in 2018.[3,4] In China, RCC incidence and mortality rates have been increasing over the past few decades, although they remain lower than those in Western countries.[5] According to recent estimates, the age-standardized incidence rate and mortality rate for RCC in China was 7.37 and 2.40 per 100,000 individuals in 2020, respectively. Clear cell renal cell carcinoma (ccRCC) is

* Corresponding authors.
E-mail addresses: qi.lin@csu.edu.cn (L. Qi), 13818585128@163.com (C. Cai), luopeng@smu.edu.cn (P. Luo), wanglinhui@smmu.edu.cn (L. Wang).
† These authors contributed equally to this work.

https://doi.org/10.1016/j.jncc.2024.06.003
Received 29 May 2023; Received in revised form 26 April 2024; Accepted 13 June 2024

the most common subtype of RCC and the pathological type of the vast majority of metastatic RCC (mRCC) cases.[6] With the development of diagnostics and surgery, early-stage ccRCC has a 5-year survival rate of up to 90% after radical surgery.[7] However, approximately 1/4 of ccRCCs are already advanced at the time of diagnosis, and approximately 1/3 of localized ccRCCs develop recurrence or metastasis after surgery.[8] Although the use of new agents (e.g., tyrosine kinase inhibitors, immune checkpoint inhibitors, etc.) has improved the prognosis of progressive or mRCC in recent years, the overall survival (OS) of these patients is still relatively short[9–11]. Therefore, further research into the molecular mechanisms underlying the progression of ccRCC and the development of new therapeutic agents remain at the forefront of current efforts to prevent and treat ccRCC.[12]

With the increasing understanding of the biological behaviors of ccRCC, the role of cell death in the pathogenesis of ccRCC and its impact on the development of new drugs are attracting the attention of researchers.[13] Cell death, including regulated and nonregulated types, plays an important role in maintaining normal body homeostasis and inhibiting the uncontrolled proliferation of tumor cells, among other biological processes.[14] Regulated cell death (RCD) consists of several types and can be genetically determined. A novel form of RCD, or cuproptosis, was recently reported in Tsvektov's study.[15] Li found that cuproptosis played a significant role in ccRCC, and remodeling analysis based on cuproptosis could successfully stratify risk classification.[16] Wang et al. revealed that the cuproptosis inducer FDX1 was correlated with tumor immunity and the prognosis of ccRCC at multiple omics levels.[17] All these findings shed further light on the mechanisms of malignant tumor initiation and progression and provide an additional theoretical basis for the search for new therapeutic strategies. Recently, Liu applied whole genome knockout technology or CRISPR-Cas9 technology and found ten hits involved in disulfidptosis.[18] Until now, there has been no comprehensive analysis of disulfidptosis in cancers, especially in ccRCC. Exploring the potential interaction between disulfidptosis and ccRCC might assist in better understanding the heterogeneity of ccRCC and provide novel diagnostic and therapeutic targets.

In this work, we depicted the aberrant expression level, biological impact, and clinical influence of disulfidptosis-related hits at the pancancer level. Next, we divided ccRCC patients into four novel subtypes based on disulfidptosis-related hits and verified them in two independent cohorts at the transcriptome and proteomic levels. DCS3, a novel ccRCC subtype with a complicated immune microenvironment, unstable genome state, and poor clinical outcome, was found in our work. Such a phenotype might be explained by its depressed disulfidptosis score. Moreover, two novel candidate agents that are sensitive to DCS3 were found and verified in our study. Taken together, we deciphered the interaction between disulfidptosis and ccRCC at the multiomics level.

2. Materials and methods

2.1. Data processing and calculation of disulfidptosis state across cancers

Transcriptome, clinical parameters, and other omics level datasets (including single nucleotide variants [SNV], copy number variation [CNV] and methylation) were downloaded from The Cancer Genome Atlas Program [TCGA] pancancer project with the use of the R package TCGAbiolinks.[19] Ten disulfidptosis-related signatures (including six synergistic and four suppressor hits) were summarized from Liu's study (Supplementary Table 1).[18] We systematically calculated the correlation of genomic mutations and the expression of ten hits by the Spearman index. The transcriptome of fragments per kilobase of transcript per million fragments mapped (FPKM) was transformed into transcripts per million (TPM) to perform further analysis. For cancer types that only possess specific omics-dimensional information or lack normal sample controls, we restrict our analysis to the characteristics of the disulfide-associated death signal at the corresponding omics level. In addition, three large ccRCC cohorts from Immotion150 (sample size = 823), Fudan University Shanghai Cancer Center (FUSCC) cohort (sample size = 133) and CPTAC-ccRCC (sample size = 133) projects, with matched transcriptome and clinical information, were adopted to perform validation analysis.[20–23] The base line information, download links of the above mentioned cohorts were summarized in Supplementary Table 2.

The index for quantifying disulfidptosis levels was established by analysing the gene expression data of core regulators of disulfidptosis, including *NUBPL, NDUFA11, LRPPRC, OXSM, NDUFS1,* and *GYS1* as positive components, and *SLC7A11, SLC3A2,* and *RPN1* as negative components. The enrichment score (ES) of gene sets that positively or negatively regulate disulfidptosis was calculated using single-sample gene set enrichment analysis (ssGSEA) in the R package GSVA. The normalized difference between the ES of positive and negative components was defined as the disulfidptosis score, allowing for computational analysis of disulfidptosis levels in tissue samples.

2.2. Identification and verification of disulfidptosis-related subtypes in ccRCC

Ten disulfidptosis hit-based expression matrices of ccRCC from TCGA-KIRC were treated as the training cohort to perform cluster analysis by ConsensusClusterPlus package.[24] The optimal cluster number was determined by consensus cumulative distribution function (CDF) and proportion ambiguous cluster number with prior knowledge. After identifying the cluster number, each subtype's biomarkers, summarized in Supplementary Table 3, from TCGA-KIRC were utilized to perform nearest template prediction (NTP) analysis among three independent ccRCC cohorts (including Immotion150, FUSCC and CPTAC-ccRCC), and the prognostic difference among three independent ccRCC cohorts was utilized to verify the reproductivity and robustness of the four disulfidptosis related subtype (DCS). NTP analysis were finished with the application of function 'runNTP' from R package MOVICS. Specifically, the most significantly differential expression gene (DEG), as determined by log2FoldChange, are selected as biomarkers for each distinct DCS subtype. These biomarkers must meet the significance threshold (adjusted $P < 0.05$) and should not be shared with any biomarkers identified for other subtypes.

2.3. Identification of genes and pathway features among subtypes

Different disulfidptosis type-related signatures, or DEGs, were determined by the DEseq2 package based on the count matrix.[25] Significant DEGs were selected with two parameters, including false discovery fates less than 0.05 and absolute fold change more than 1.8. Visualization of DEGs and disulfidptosis genes was performed by the Complexheatmap package. Accordingly, the biological annotation behind DEGs was analysed by the package with the aid of Msigdb datasets.[26,27] ESs of pathways from the packages MOVICS and IOBR were calculated by the package GSVA.[28] Transcriptome factor activation scores were quantified with the use of the R package RTN based on transcriptome matrix.[29,30]

2.4. Correlation of disulfidptosis and tumor microenvironment components in ccRCC

We quantified immune cell- and component-related signature scores by the single-sample GSVA algorithm.[31] Seven antitumour step scores of antitumors were downloaded from the TIP database.[32] We calculated the correlation of the expression level of immune genes and immune gene set signatures extracted from the IOBR and MOVICS packages.[28] The degree of immune cell infiltration was quantified by seven deconvolution algorithms. The R package estimate was adopted to evaluate three scores, including stromal, immune and ESTIMATE scores.[33] The vessel normalization score was calculated by the ratio of pericytes to the endothelial cell score of each sample, which has been reported in previous work.[34]

2.5. Genomic and drug sensitivity between subtypes

The SNV information and tumor mutation burden (TMB) calculation of TCGA-KIRC were performed by the Maftools package.[35] Genome amplification and deletion events were calculated with application of GISTIC software.[36] For mutation frequency and cooccurrence events, the inner function from Maftools was adopted. Therapy response information from the Genomics of Cancer Drug Sensitivity (GDSC), Connectivity Map (CMAP) and profilingrelative inhibition simultaneously in mixtures (PRISM) databases was downloaded to detect potential potent agents for different types, especially for DCS3.[37] The half maximal inhibitory concentration (IC50) of each cluster was calculated and compared by the R package pRRophetic.[38]

2.6. Impact of NU1025 on ccRCC cell malignancy

NU1025 (id: S773001) was purchased from Selleckchem. The optimal concentration of 500 nM was used according to the instructions. We selected the DCS3-related cancer cell line A704 by the NTP algorithm from the Cancer Cell Line Encyclopedia (CCLE) database and used A704 to perform *in vitro* experiments. Transwell, migration, colony formation, and wound healing experiments were applied to detect the inhibitory effect of NU1025. The detailed experimental details have been introduced and summarized in our previous works.[39–41] Each experiment mentioned above was performed three times independently.

2.7. Statistical analysis

All data cleaning, results visualization, and statistical comparison were performed in R and SPSS software. Comparisons of continuous variables were performed with *t* tests or Kruskal–Wallis or ANOVA tests. Categorical variables were compared by the *chi-square* test. Cancer- and metabolism-related signatures were analysed with the aid of the packages MOVICS and IOBR.[42] Visualization of disulfidptosis-related genes at multi-omics level was performed by the GSCA website.[43,44] Kaplan–Meier curves were plotted by survival and survminer packages. *P* values and false discovery rate (FDRs) less than 0.05 were considered significantly different. More analysis details can be seen in our previous studies.[45–48]

3. Results

3.1. Dysregulation of disulfidptosis-related genes across cancers

The overall strategy of this study is summarized in Supplementary Fig. 1. Since cell death-related signatures play a pivotal role in cancer progression, we first analysed the expression and disulfidptosis level, prognostic impact, methylation, CNV and SNV among cancers. As Figs. 1A and B showed, nearly ten disulfidptosis signatures, except *SLC7A11*, were downregulated in tumor tissues compared with normal tissues; *SCL7A11* was most highly expressed in cholangiocarcinoma (CHOL) among all cancer types. Regarding the prognostic impact of disulfidptosis-related signatures, all normal genes displayed risky roles when analysing OS and progression free interval (PFI) (Fig. 1C). Interestingly, the prognostic impact of *NUBPL, LRPPRC, OXSM, NDUFS1* and *NCKAP1* was protective in kidney renal clear cell carcinoma (KIRC) (Fig. 1C). After calculating the disulfidptosis score in each cancer type, we found that most tumor tissues led to a depressed disulfidptosis state compared with normal tissues, except glioblastoma (GBM), as shown in Fig. 1D. We also analysed the DNA methylation level of the ten hits and found that the deregulated expression state of most signatures was significantly negatively correlated with methylation, especially in *SLC7A11* and *RPN1* (Fig. 1E). In addition, we noticed that the mutation frequency of *LRPPRC* was highest among the ten hits, and *UCEC* was ranked as the hottest musted type among all cancers (Fig. 1F). Finally, we observed that the most common types of CNV among the ten hits were heterozygous amplification and deletion, and this phenomenon was especially noticeable in the *OXSM* and *RPN1* genes and in *ACC, UCS, LUSC, HNSC* and *OV* (Fig. 1G).

3.2. Biological implication of disulfidptosis in cancers

To better understand the potential biological roles of hits of disulfidptosis, we investigated the correlation between classical cancer hallmarks, immune processes and disulfidptosis score. Notably, a negative correlation index was found among TNFα signaling via NFκB, KRAS, interferon γ and α, inflammation, IL6-JAK-STAT3 and epithelial mesenchymal transition (EMT) and disulfidptosis score, while a positive correlation was found between oxidative phosphorylation and disulfidptosis (Fig. 2A). Fig. 2B showed a significant correlation between disulfidptosis and immune components, which was found to stimulate infiltration of neutrophils, Th17 cells, Tregs, effector memory cells and monocytes while inhibiting CD4 T cells, Tfh cells, NK cells, CD8 T cells, gamma delta T cells and cytotoxic cells in cancers. The datasets from starBase, microde and mirnet implicated the ceRNA network of *SLC7A11* and *NCKAP1*, which suggested that AC093010.3-has-miR-27a-3p-SLCA11, AC103702.1-has-miR-122-5p-SLCA11 and has-miR-34c-3p-NCKAP1 might contribute to the dysregulation of *SLCA11* and *NCKAP1* among cancers (Fig. 2C). The results from Genemania revealed the potential interaction of ten hits with other genes, such as *SLC7A10, NUBP2, KDM5* and *SLC1A7* (Fig. 2D). The results from the GSCA database showed that most disulfidptosis hits were positively correlated with apoptosis, the cell cycle and the DNA damage pathway but negatively correlated with EMT (Fig. 2E). Regarding the drug sensitivity of hits, the results from the GDSC database postulated that *LRPPRC* was positively related to dasatinib, temsirolimus, AZD6482, and BEZ235, while *GYS1* was nearly negatively correlated with all drugs, especially TGX221, MG-132 and AZ628 (Fig. 2F). Furthermore, Fig. 2G showed that high expression of *NCKAP1, SLC7A11* and *GYS1* resulted in sensitivity to nearly all drugs in The Cancer Therapeutics Response Portal (CTRP), while LRPPRC led to a reverse correlation.

3.3. Different disulfidptosis-related subtypes displayed distinctive clinical outcomes

As we found above, nearly all disulfidptosis-related genes were protective factors for ccRCC (Fig. 1C) and disulfidptosis scores were significantly depressed in tumor tissues (Fig. 1D), which was unique and different from other cancers. Thus, we investigated the role of the ten disulfidptosis hits in ccRCC. The CNV frequency of ten hits differed, and *OXSM* displayed the highest genome loss rate, while *NCKAP1* had a higher genome gain frequency (Fig. 3A). The total mutation frequency of ten hits was lower in ccRCC, which ranked as *LRPPRC, NDUFS1, SLC3A2* and *OXSM* (Fig. 3B). In the whole expression landscape of ccRCC, we noticed that *SLC3A2, OXSM, NUBPL, NDUFS1, LRPPRC* and *NCKAP1* were more highly expressed, while *NDUFA11, SLC7A11, GYS1* and *RPN1* were less expressed in normal tissues (Fig. 3C). Univariate Cox analysis further showed the protective roles of disulfidptosis hits in ccRCC and suggested three expression relation patterns of ten hits (Fig. 3D). Fig. 3E revealed the expression correlation of ten hits, and we found that *LRPPRC* and *NCKAP1* had the most significant positive correlation, while *NUBPL* and *NDUFA11* had a negative relationship in ccRCC. We next applied cluster analysis of ccRCC to better understand the role of disulfidptosis in ccRCC, and we chose 4 as the optimal subtype number (Supplementary Fig. 2A-D). We found that the prognosis of DCS4 was superior to that of the other types in both OS and PFI, as shown in Fig. 3F. The expression level of ten hits also varied across four types and normal renal tissues, and we defined DCS3 as the disulfidptosis cold subtype, DCS1 as the disulfidptosis hot subtype, and DCS2 as the mixed or disulfidptosis relative cold subtype (Fig. 3G). Compared with DCS1, the other three subtypes had poor clinical characteristics, such as T, N,

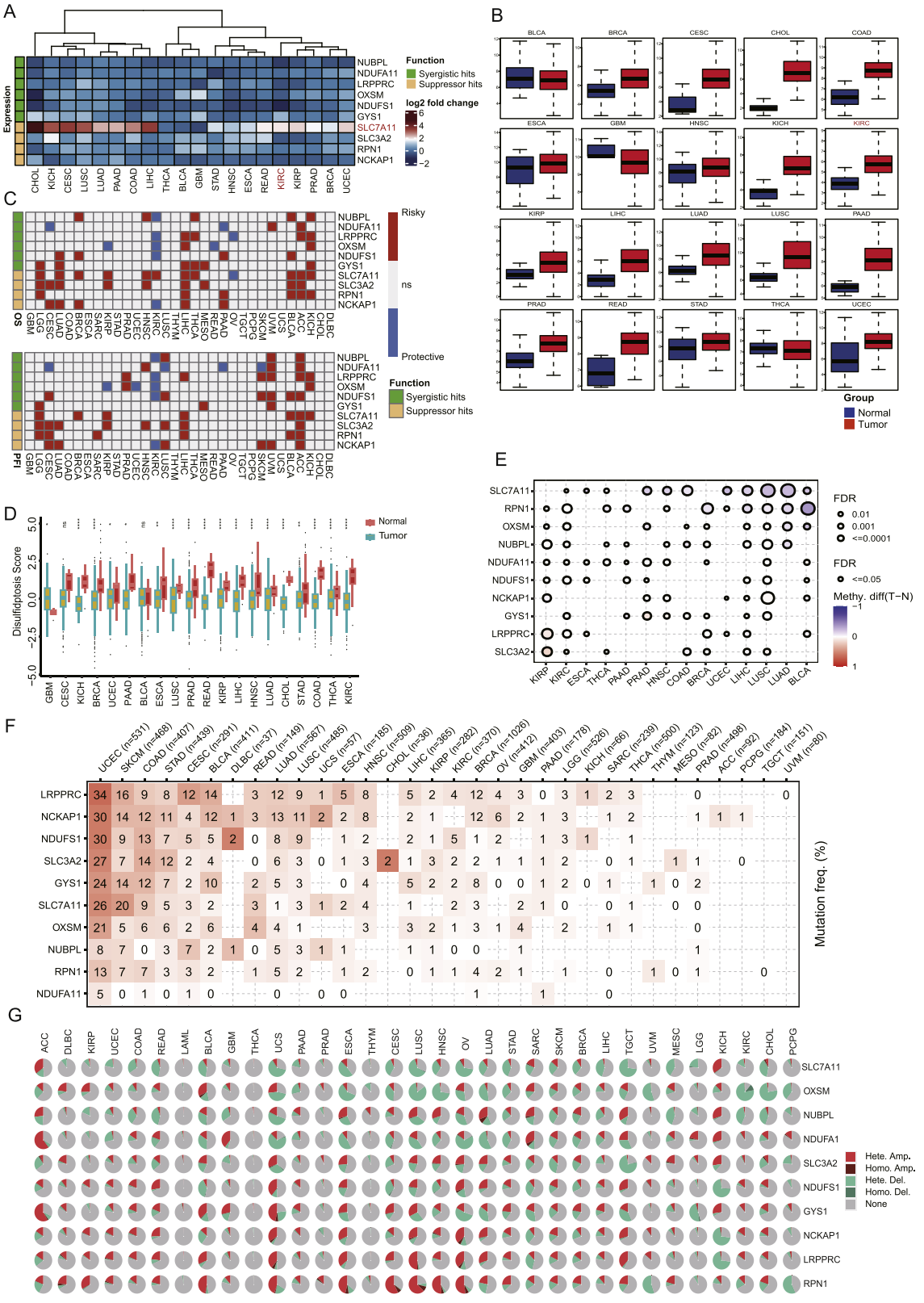

Fig. 1. Multiomics futures of disulfidptosis among pancancer. (A) Expression difference of ten disulfidptosis hits between tumor and normal tissue across pancancer. Red represents higher expression in tumor tissues, while blue represents lower expression levels. (B) SLC7A11 expression in normal (blue) and cancer (red) tissues. (C) Prognostic impact of disulfidptosis hits in various cancers. The upper panel represents the prognostic impact on OS, and the lower represents PFI. (D) Disulfidptosis score calculated by ssGSEA difference between normal and tumor tissues. (E) Methylation difference of ten disulfidptosis hits; purple represents hypermethylation, while orange represents hypomethylation. (F) Single-nucleotide variants of ten hits; a deeper color represents a high frequency of mutation. (G) Pie plot indicating copy number variation of ten disulfidptosis hits. The types of copy number variation are illustrated on the left. Amp, amplification; Del, deletion; FDR, false discovery rate; Freq, frequency; Hete, heterogeneity; Homo, homogeneity; Methy.diff, methylation differentiation; N, normal; OS, overall survival; PFI, progression-free interval; T, tumor; ns, not significant.

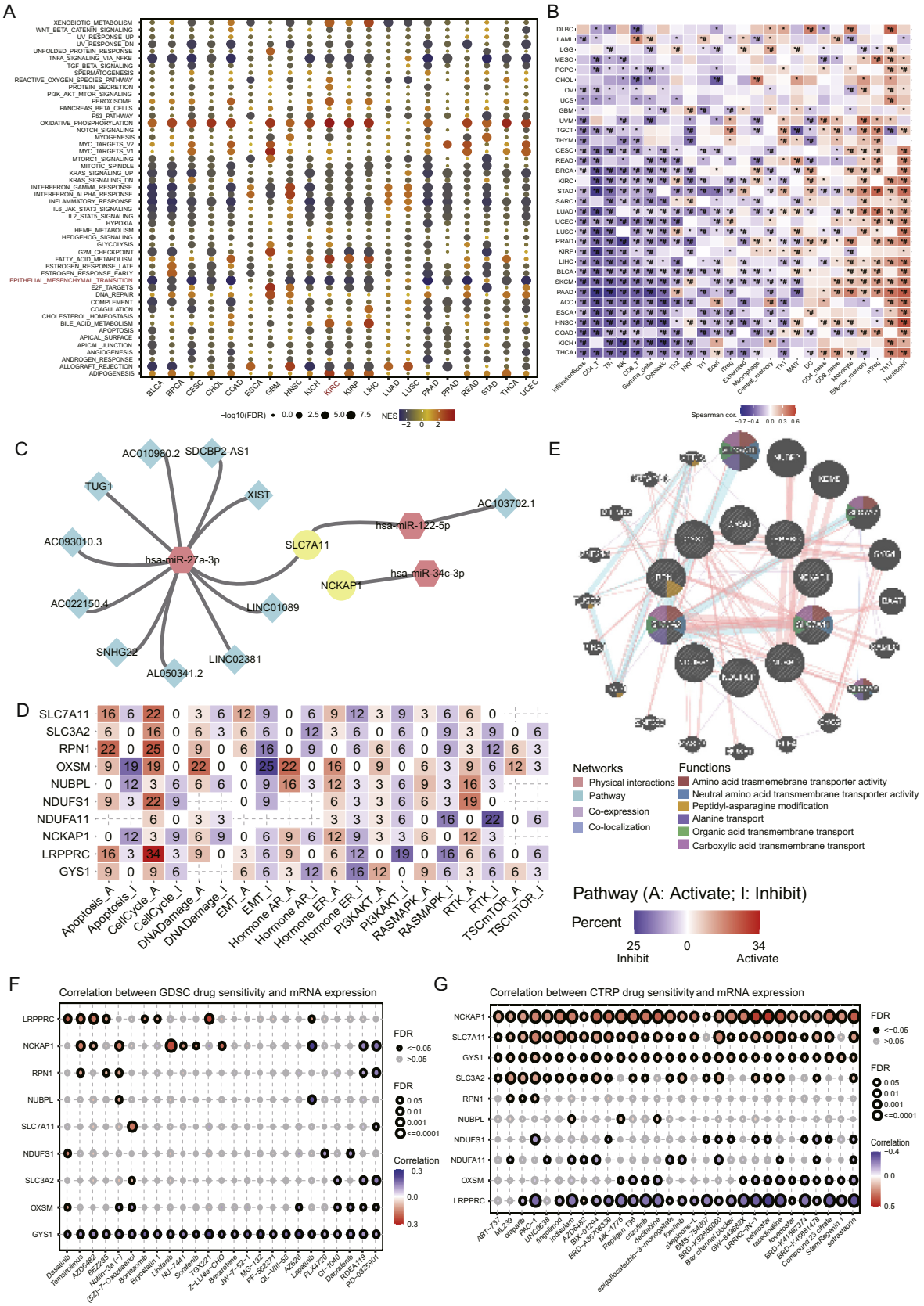

Fig. 2. Characteristics of ccRCC and subtype or risk score. (A) GSEA of cancer hallmark enrichment scores between high and low disulfidptosis score subtypes. (B) Correlation of disulfidptosis score and immune signatures among cancers. Orange represents a positive correlation, while purple represents a negative correlation. (C) ceRNAs of lncRNAs (blue), miRNAs (red) and mRNAs (yellow) of disulfidptosis hits. (D) Gene interaction of ten hits from Genemania. (E) Correlation of disulfidptosis score and classic cancer pathway score. The total effect of each hit was the activated score minus the inhibited score. (F, G) Correlation of drug sensitivity and ten hit expression levels from the GDSC (F) and CTRP (G) databases. FDR, false discovery rate; NES, normalized enrichment score. *, $P < 0.05$; #, false discovery rate < 0.05.

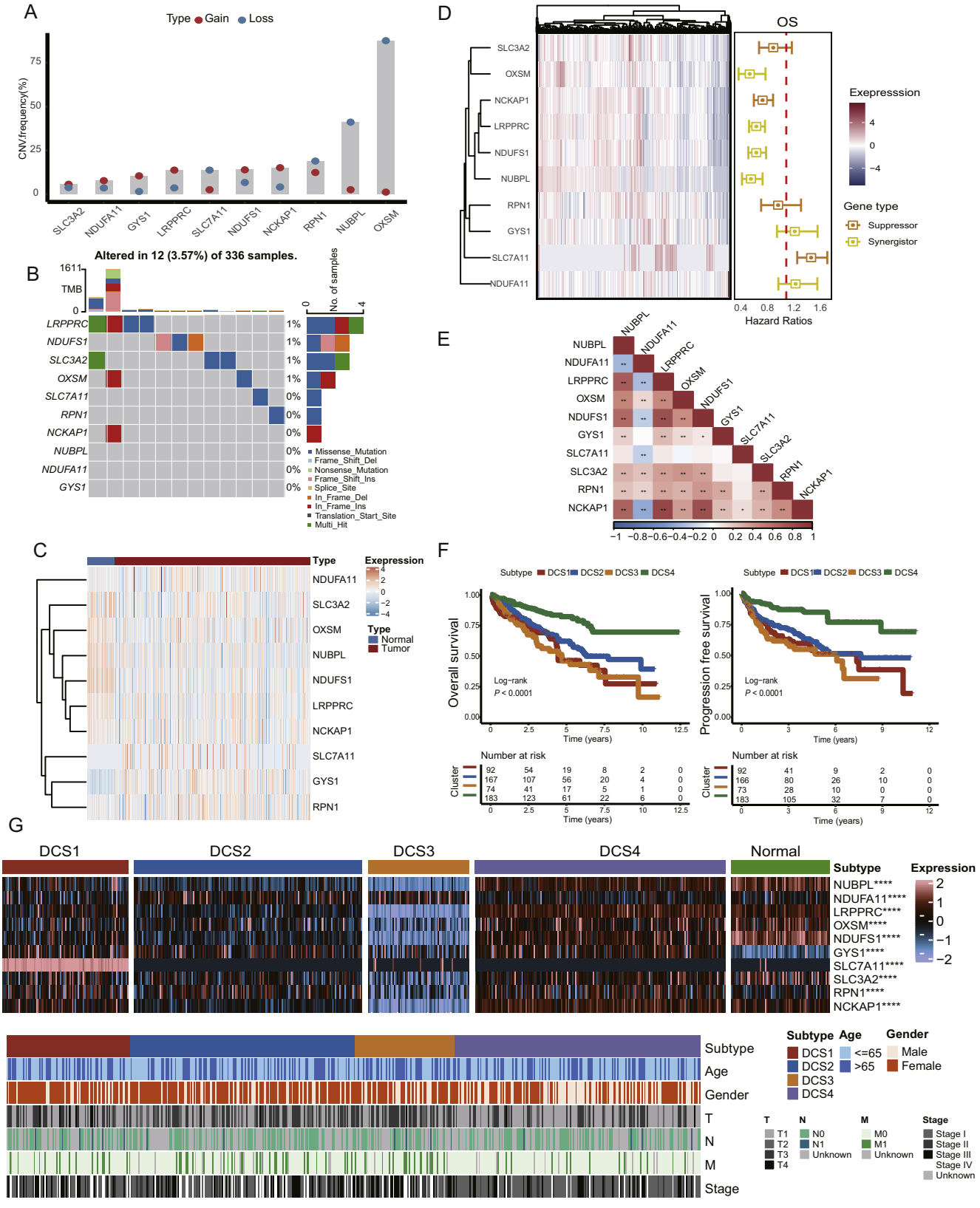

Fig. 3. Association of subtype in ccRCC based on disulfidptosis hits. (A) Lollipop chart showed the CNV copy number variation of ten hits in ccRCC. (B) The waterfall plot depicted the mutation landscape of disulfidptosis genes in TCGA-KIRC, altered in 12 (3.57%) of 336 samples. (C) Heatmap indicated the expression differences in tumor and normal tissues from TCGA-KIRC. (D) Heatmap and forest plot illustrated the expression pattern and OS of ten hits by univariate Cox analysis. (E) Correlation of the expression of ten hits. Red represents a positive correlation, while blue represents a negative correlation. (F) Overall survival and progression free survival analysis of four subtypes in ccRCC. (G) Heatmap illustrated the different expression levels of disulfidptosis hits among subtypes and normal tissues (upper panel) and clinical characteristics of different disulfidptosis subtypes (lower panel). CNV, copy number variation; Del, deletion; Ins, insertion; OS, overall survival; TMB, tumor mutation burden; *, $P < 0.05$; **, $P < 0.01$; ****, $P < 0.0001$.

M and stage (Fig. 3G). We adopted three independent ccRCC cohorts at the transcriptome and protein levels from previous works and utilized NTP to perform cluster analysis. The results showed that DCS3 in both cohorts led to a poor prognosis, which proved the applicability and robustness of the cluster results based on disulfidptosis hits (Supplementary Fig. 2E and F, Supplementary Table 4).

3.4. Distinctive biological and transcriptome factor regulon differences

To decipher the biological differences among the four types, we next performed gene expression analysis. The DEGs of four subtypes were annotated on several classic GO terms of ccRCC. In detail, we found that keratinization and negative regulation of apoptosis execution were activated in DCS3, while the Hippo signal was activated in DCS4. The downregulated DEGs also showed such biological differences (Figs. 4A and B). Further analysis revealed that DCS4, with the best prognosis, displayed a depressed state of several immune-related signals, including interleukins, cytokines, the TNF superfamily, cell functions, B and T-cell function, and chemokines (Fig. 4C). We also verified such differences in the MOVICS package and found that several classic cancer pathways, including EMT, MDSCs, immune checkpoints, CD8 T-cell exhaustion, Tregs and plasmacytoid dendritic cells (pDCs), were downregulated in DCS4, while those signals were activated in the other cancer subtypes (Fig. 4D). We also noticed several specific activated transcriptome regulators in DCS3, including PITX2, HOXA13, SHOX2, ZIC2, DMRT3, and HOXB13, and depressed transcriptome regulators, including ZEB2, ZNF93, TFE3, TP53, E2F1 and FOXM1 (Fig. 4E). We also found that several hallmarks were downregulated in DCS3, including the G2M checkpoint, E2F, PI3K-AKT-MTOR, protein secretion, and mitotic spindle, while kras signaling was activated (Supplementary Fig. 3A). Specifically, Supplementary Fig. 3B showed that inositol phosphate metabolism, ADP ribosylation, glycogen biosynthesis and degradation, and hexosamine biosynthesis were depressed in DCS2.

3.5. DCS3 exhibited an immune dysfunctional state among subtypes

We noticed that several immune stimulators were lower in DCS3, such as BTN3A1, CXCL9, CXCL10, EDNRB and several antigen presentation genes, which might be explained by the dysregulated state of DNA methylation and genome mutation (Fig. 5A). Consistently, we noticed that the CD8 T effector score was highest in DCS3, while mismatch repair, nucleotide excision repair, DNA damage response (DDR) and DNA replication scores were lowest in this type (Fig. 5B). In addition, we noticed that DCS3 had the lowest stromal score and highest immune score among the four types (Fig. 5C). We next applied the TIDE algorithm to compare the antitumour potency among the four types, and we observed that the TIDE and immune dysfunction scores were higher in DCS3, while the immune exclusion score was lowest in DCS3 (Fig. 5D). The MSI signature score also varied among the four types (Fig. 5D). The CYT score distribution also proved the antitumour deficiency of DCS3 (Fig. 5E). When estimating the immunotherapy response (Fig. 5F), we found that DCS3 showed a lower response rate (26%) than the other types (DSC1: 37%, DCS2: 31%, DCS4: 42%). We noticed that DCS3 had an immune cold phenotype in the TIMER algorithm, and neutrophil and M2 cell signals were consistently lower across different immune algorithms (Supplementary Fig. 4A).

When we compared differences in TIP, we found various activated states among the four ccRCC subtypes. In detail, DCS1 showed relatively low scores for cancer antigen release and presentation, which might help explain the relatively depressed antitumour immunity (Supplementary Fig. 4B). We also found that cancer-associated fibroblasts (CAF) scores and vessel normalization scores were lowest in DCS3 (Supplementary Fig. 4C). In addition, we also compared the immune-related gene expression levels among subtypes, which also showed a complicated immune state, among which several chemokines and receptors were downregulated in DCS3, while most immune inhibitors and stimulators were expressed at lower levels in DCS4 (Supplementary Fig. 5A). Furthermore, we observed that nearly all immune checkpoint inhibitor (ICI) regulators were downregulated in DCS4; consistently, all immune cells were minimally infiltrated in DCS4, except endothelial cells (Supplementary Fig. 5B).

3.6. DCS3 led to the most unstable genome structure compared with the other types

In total, we found that DCS4 had a lower mutation rate (82.79%) than the other three types (DCS1: 89.47%, DCS2: 90.29%, DCS3: 89.47%), as shown in Fig. 6A. Such a difference was obvious when comparing DCS3 with DCS4 on chromosomes 3, 5 and 7 (Fig. 6B). Detailed information on the genome can be found in Supplementary Fig. 6. The genome alteration frequency of DCS3 was the highest, and that of DCS4 was the lowest (Fig. 6C). We also noticed a higher TMB rate in DCS3, even though the difference was not significant (Fig. 6D). In addition, we noticed that RTK–RAS, PI3K and Hippo signals displayed a lower mutated frequency when compared with the remaining subtypes (Supplementary Fig. 7A). We also detected significantly different mutation interaction landscapes among the four types, and *NALCN-TTN, NALCN-PTEN, KDM5C-TTN*, and *SETD2-PBRM1* cooccurred in DCS2, while *ABCB1-BAP1* and *MTOR-BAP*1 cooccurred in DCS4 (Supplementary Fig. 7B).

3.7. Tumor cell lines belong to DCS3 were sensitive to lisitinib and NU1025

Considering the malignant phenotype of DCS3, we retrieved different drug databases to identify subtype-specific agents, especially for DCS3. We observed that DCS3 led to paradigmatic resistance to target agents, including axitinib, crizotinib, erlotinib, imatinib, pazopanib, saracatinib, temsirolimus, afatinib, erlotinib and sunitinib, while sensitizing to lisitinib (Fig. 7A). In addition, we detected several potential agents for DCS3 according to the IC50 value, which consisted of CI1040, SL01011, PD0325901, Nutlin3a, LFMA13 and gefitinib (Fig. 7B). Furthermore, datasets from CMAP suggested that NU1025 might also work in DCS3 according to its lowest CMAP score (Fig. 7C). After identifying DCS subtype-related cell lines from GDSC with the use of the NTP algorithm, we next performed *in vitro* experiments to evaluate the therapeutic effect of NU1025 on A704 and 786p (Fig. 8A). When A704 and 786P cells treated with NU1025 at 500 nM concentration, the prefiltration, migration and invasion abilities were significantly inhibited, which suggested that patients clustered into DCS3 might be sensitive to NU1025 (Figs. 8B-E).

3.8. SLC7A11 was correlated with the malignant phenotype of ccRCC

Radom forest analysis suggested that SLC7A11 ranked as the most prognosis-relevant gene among the ten hits (Fig. 9A). Univariable Cox analysis revealed that SLC7A11 functioned as a risk factor for the OS of the GSE167573 cohort, OS of E-MTAB-1980, OS of TCGA-KIRC, disease specific survival (DSS) of TCGA-KIRC and progression free survival (PFS) of TCGA-KIRC. KM curves also showed that the SLC7A11 high expression group had a short survival time (Fig. 9B). We found that the SLC7A11 expression level was high in tumor tissues, and its expression level was higher in the later T and grade subgroups (Fig. 9C and D). SLC7A11 expression levels were also correlated with several clinical parameters, including Karnofsky performance score, lactate dehydrogenase result and platelet qualitative result (Fig. 9E). At the single-cell level, we noticed that SLC7A11 was more highly expressed in the plasma and pDC clusters in GSE145281 and GSE139555, respectively (Fig. 9F). The GO term suggested that SLC7A11 might be mainly involved in de novo protein folding, integrated stress response signaling, noncoding RNA 3 end processing, etc. (Supplementary Fig. 8A). GSEA ranked the most potentially impacted pathways as the E2F target, MTORC1 and G2M checkpoint pathways (Supplementary Fig. 8B). We

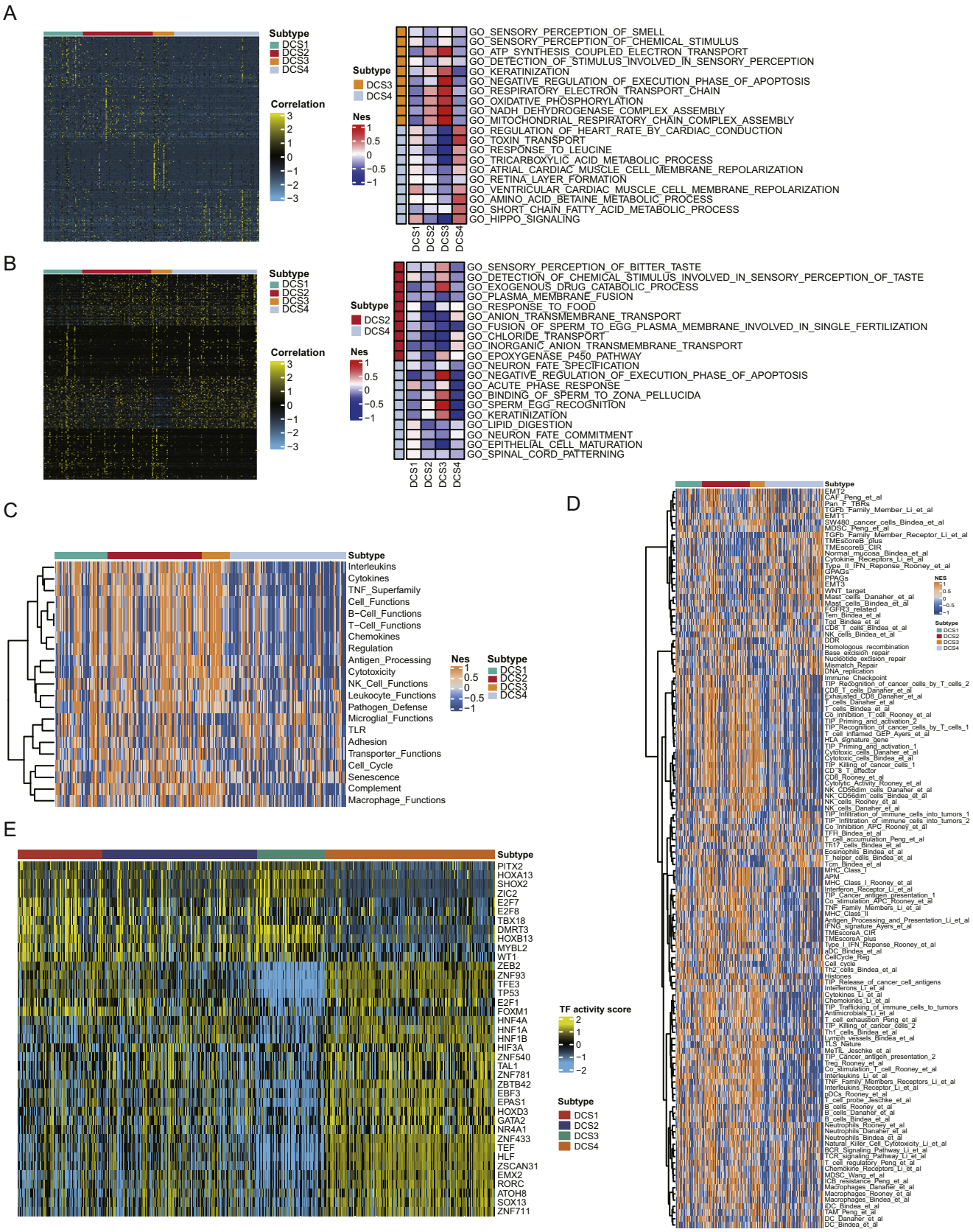

Fig. 4. Biofunction of DEGs among the four subtypes. (A) The left heatmap indicated the upregulated DEGs among the four types, and the annotation of upregulated DEGs was depicted in the right heatmap. (B) Left heatmap indicated downregulated DEGs among the four types, and annotation of downregulated DEGs was depicted in the right heatmap. (C, D) Heatmap presented different cancer-related signal scores and immune-related signature scores among the four subtypes. (E) Heatmap showed different activation scores or regulons of ccRCC-related transcriptome factors among the four types. DEGs, differential expression genes.

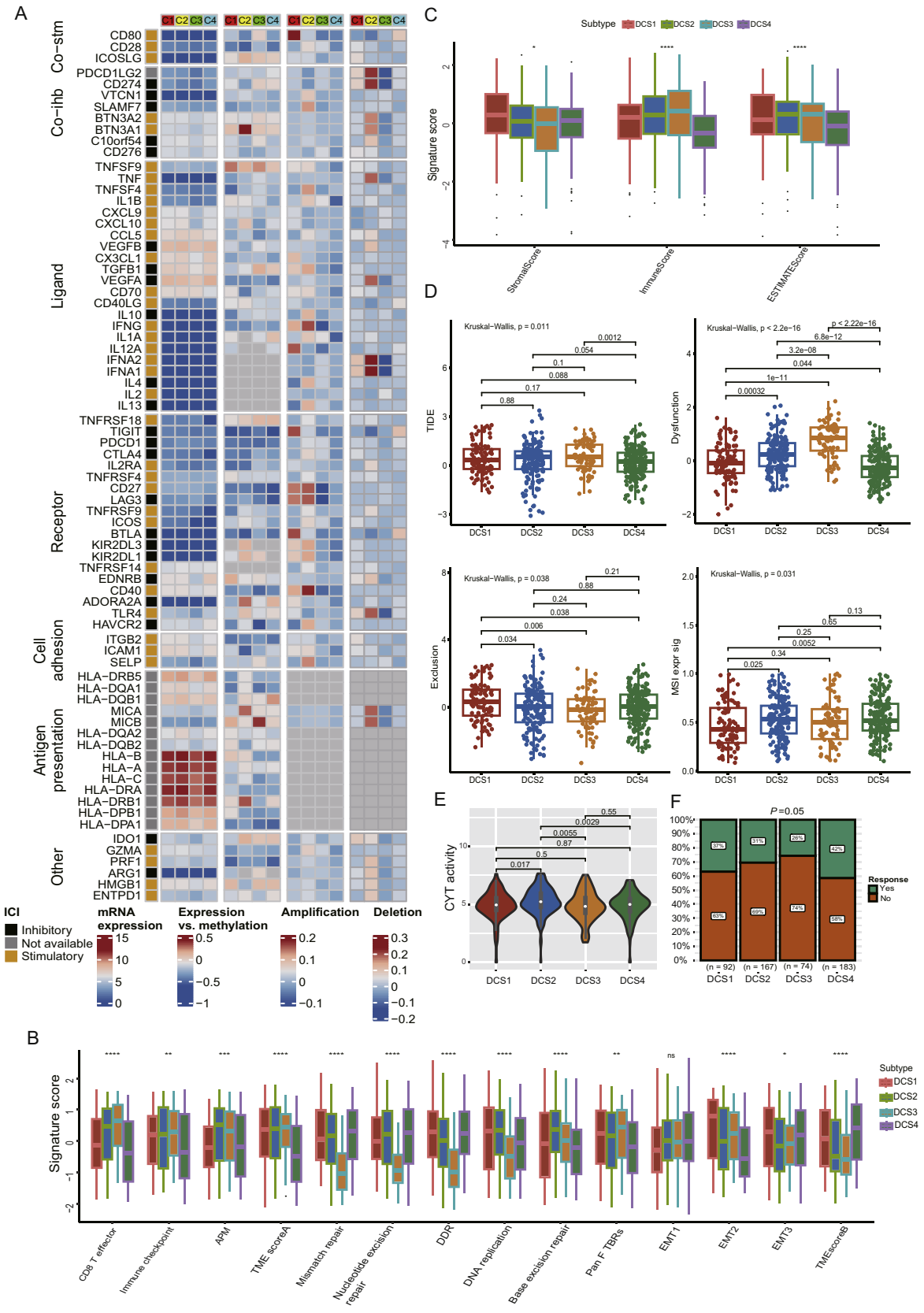

Fig. 5. Immune landscape of different disulfidptosis subtypes in ccRCC. (A) Heatmap showing the expression pattern and impact of methylation, amplification, and deletion frequency on immune genes among different subtypes. DCS1, red; DCS2, yellow; DCS3, green; DCS4, blue. (B) Boxplot showed different immune signature scores among subtypes. (C) Boxplot indicated stromal, immune and ESTIMATE scores among subtypes. (D) Boxplot combined with scatter plot depicting the TIDE, immune dysfunction, exclusion and MSI score among subtypes. (E) Violin plot postulates CYT score among subtypes. (F) Column scale chart of ICI response differences among subtypes. Co-inh, co-inhibitor; Co-stm, co-stimulator; CYT, cytolytic activity; ICI, immune checkpoint inhibitor; MSI, microsatellite instability; TIDE, tumor immune dysfunction and exclusion; ns, not significant; *, $P < 0.05$; **, $P < 0.01$; ***, $P < 0.001$; ****, $P < 0.0001$.

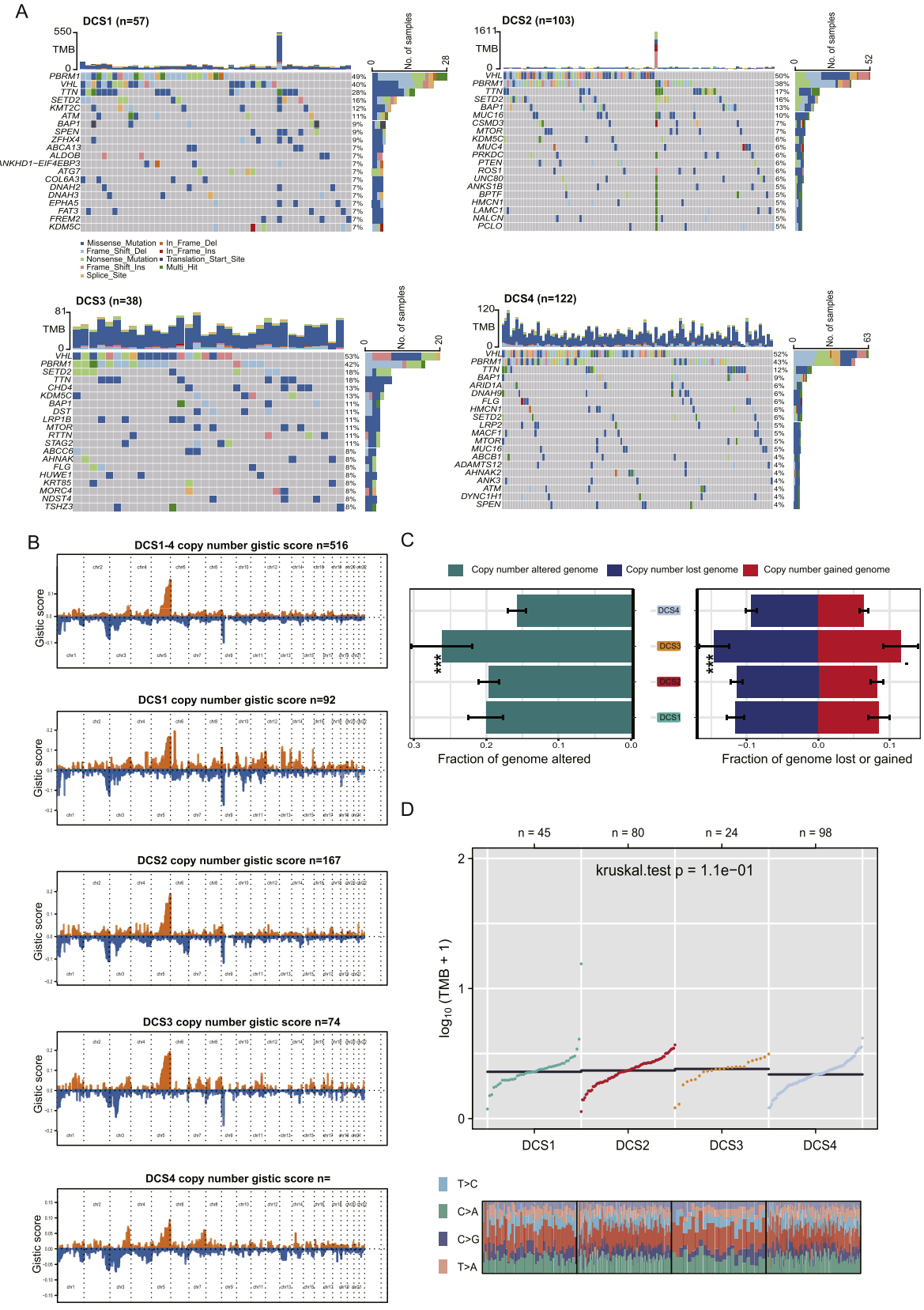

Fig. 6. Mutation profile and TMB of four subtypes. (A) Waterfall plot illustrated the mutation characteristics of four ccRCC subtypes. DCS1 (89.47%, top left), DCS2 (90.29%, top right), DCS3 (89.47%, low left), DCS4 (82.79%, lower right). (B) Mutation details of four types of chromosomes, orange represented genome gain, while blue represented genome loss. (C) Barplot quantified the total copy number variation in DCS1, DCS2, DCS3 and DCS4. (D) Scatter plot indicated the TMB differences among the four types. Del, deletion; Ins, insertion; TMB, tumor mutation burden; ***, $P < 0.001$.

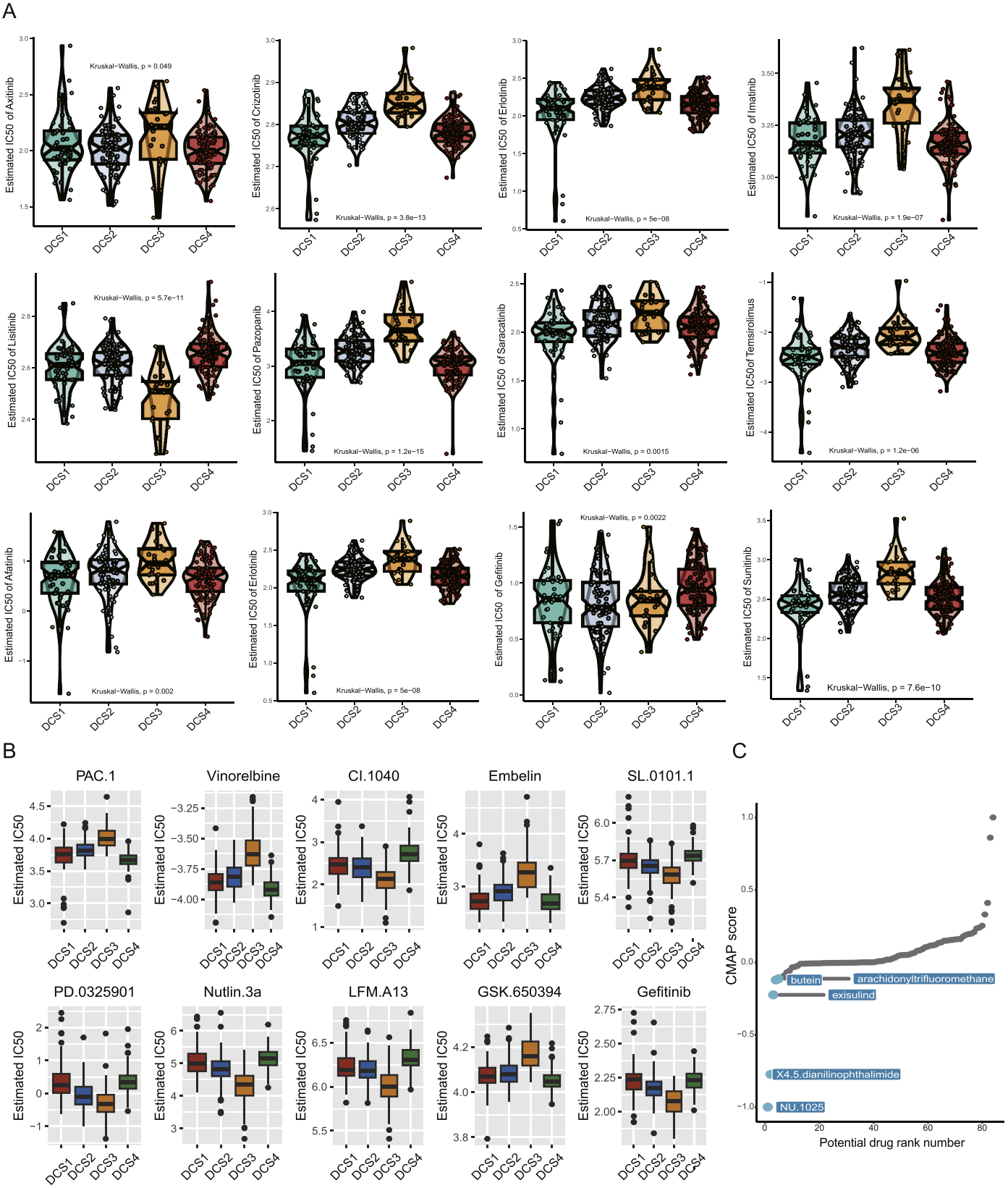

Fig. 7. Drug sensitivity and potential agents for different subtypes. (A) Box-violin plots showed different therapeutic sensitivities among the four subtypes. The x-axis showed different subtypes, and the y-axis represented the estimated IC50 values of different agents. (B) Boxplot indicated the top 10 different IC50 values of drugs from the GDSC database. (C) Scatter plot showed CMAP scores of different agents from the Cmap database. The lower Cmap scores suggested the high sensitivity for DCS3. IC50, half maximal inhibitory concentration.

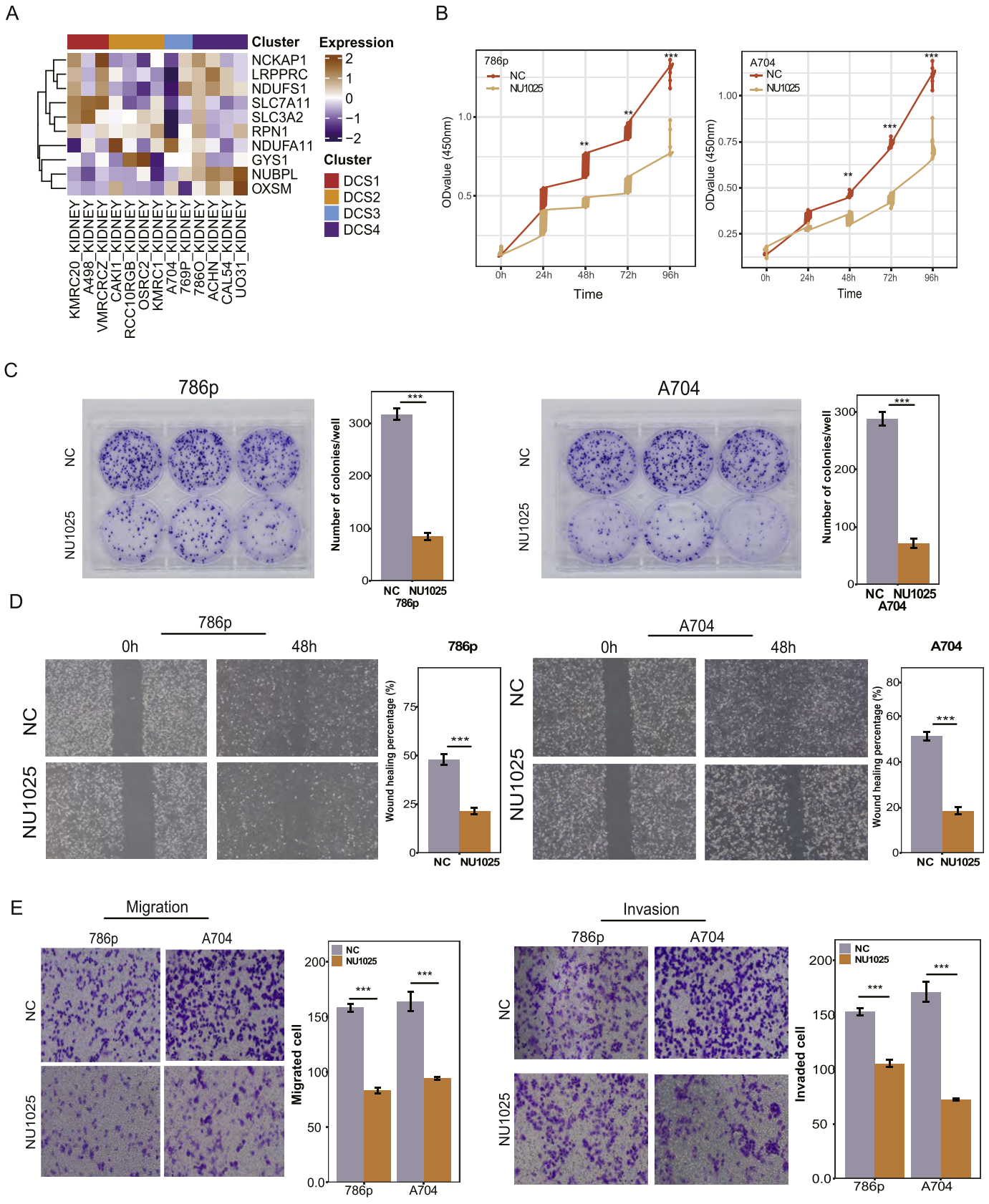

Fig. 8. Addition of DU1025 could inhibit ccRCC progression. (A) Nearest template prediction analysis of the expression matrix of ccRCC cell lines from CCLE based on biomarkers from four subtypes. (B, C) Different proliferation ability of ccRCC cell in CCK8 kit and (C) clone formation. (D) Wound healing experiments showed difference migration ability of different groups. (E) Migration and invasion assays of 786p and A704 treated or not treated with NU1025. NC, negative control. **, $P < 0.01$; ***, $P < 0.001$.

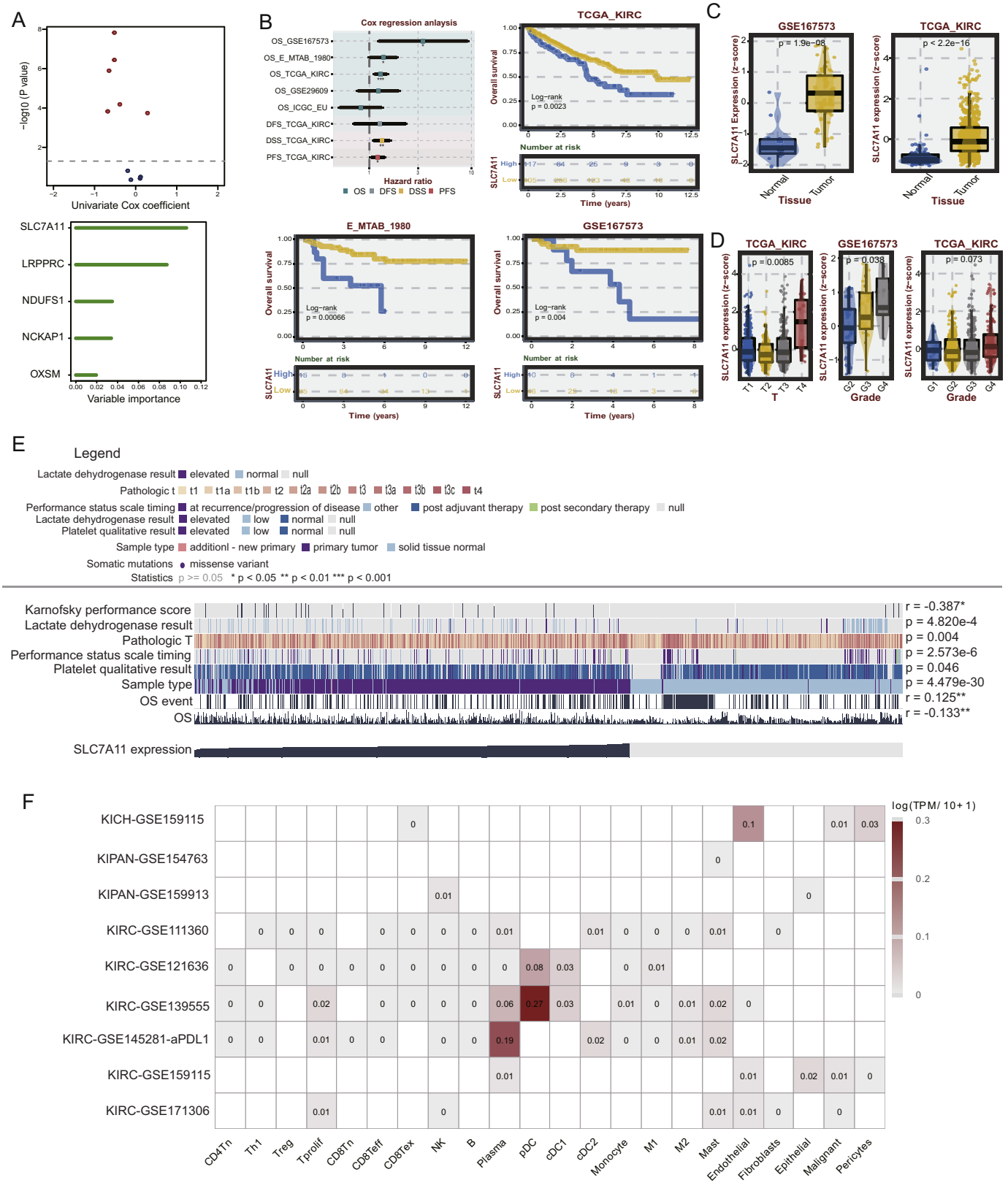

Fig. 9. Important role of SLC7A11 in ccRCC. (A) Volcano plot showed the prognostic values of ten hits. The X-axis showed the univariable Cox coefficient, while the y-axis shows -log10 (*P* value); Red points represent gene with *P* value < 0.01, blue points represent gene with *P* value > 0.05. (B) Cox regression and KM analysis of SLC7A11 in multiple ccRCC datasets with different clinical outcomes. (C) SLC7A11 expression level in normal and tumor renal tissues from the GSE167573 and TCGA-KIRC cohorts. (D) Expression level of SLC7A11 in different T stages and grades of ccRCC. (E) Correlation of SLC7A11 expression and clinical parameters in the TCGA-KIRC cohort. (F) Different expression levels of SLC7A11 at the single-cell level across ccRCC cohorts. DFS, disease free survival; DSS, disease specific survival; PFS, progression free survival; OS, overall survival; TPM, transcripts per million. *, $P < 0.05$; **, $P < 0.01$; ***, $P < 0.001$.

also divided all ccRCC patients into low SCL7A11 and high SCL7A11 subtypes based on the median expression level and found that PBRM1 and chrome3 gain events had a higher mutation frequency in the latter group, which could help explain the aberrant expression level of SLC7A11 in ccRCC (Supplementary Fig. 8C). Considering the higher expression level of SLC7A11 in ccRCC patients, we found several potential agents targeting the SLC7A11 group in ccRCC, including temozolomide, bicalutamide, bosutinib and lenalidomide (Supplementary Fig. 8D).

4. Discussion

Resistance to cell death is an important feature of tumors, and the induction of tumor cell death is an important pathway for the efficacy of combined therapy, which can be synergistic with other therapies, including targeted therapies and immunotherapies.[49] Programmed cell death (PCD), or RCD, not only plays a key role in development and cellular homeostasis, but its dysregulation is closely associated with many diseases, including inflammation and cancer.[50] PCD, including scorch death, pyroptosis, autophagy, and necroptosis, is a central area of research to unravel resistance to tumor cell death, as it is regulated by specific molecular pathways and can be targeted by genetic or pharmacological means.[51] PCD and immunotherapy are closely linked, with the latter acting as inducers of programmed death in which $CD8^+$ T cells inhibit tumor growth by inducing tumor cells to undergo necrosis, pyroptosis and ferroptosis.[52] Approximately two-thirds of ccRCC patients do not respond to immunotherapy due to defective release of tumor antigens caused by cell death resistance.[53] Inflammatory factors and specific antigens released by tumor cells induced by PCD can turn cold tumors into hot tumors, which in turn recruit immune killer cells, including NK and $CD8^+$ T cells. Recently, the combination regimen of BRAF and MEK inhibitors (BRAFi+MEKi) was shown to recruit $CD4^+$ and $CD8^+$ cells by inducing tumor cells to undergo scorch death, which in turn induces dendritic cell maturation.[9] T-cell infiltration exerts an antitumour immune effect, and this regimen has been approved by the FDA for the treatment of melanoma with BRAF V600E/K mutations.[51] However, programmed death can also have pro-cancer effects in certain cancers, and Demuynck et al. found that ferroptosis in breast cancer cells increased oxidized lipid levels in the microenvironment, leading to reduced phagocytosis and antigen cross-presentation by dendritic cells, which helped tumor cells evade immune surveillance.[54] In conclusion, PCD and antitumour immunity are inextricably linked; the specific roles played by different types of PCD in tumors can be anticancer or pro-cancer, depending on the heterogeneity of the tumor itself and the regulatory mechanisms after cell death.

Recently, Li and colleagues observed a novel form of RCD, which is more common in SLC7A11 high expression cancer cell lines, and they finally defined it as disulfidocytosis.[18] In detail, when performing glucose starvation in SCL7A11 high-expressing cells, aberrant disulfide bonds could form in the framework of actin cytoskeleton proteins and finally simulate the collapse of F-actin. In contrast to traditional ferroptosis and apoptosis, one of the typical features is aberrant accumulation of intracellular disulfides. Considering the paradigmatic high expression of SCL7A11 in solid tumours, targeting disulfidptosis in the integrated treatment of cancer is regarded as a valuable strategy. Growing evidence suggests that inducing cancer cell death can inhibit cancer progression by limiting the cancer cell itself but also reshaping the tumor microenvironment. Our previous work found that inducing renal cell cuproptosis could enhance antitumour immunity by activating cGAS-STING-TBK1 signaling in dendritic cells, which promoted the efficacy of immune checkpoint inhibitor therapy in a C57BL mouse model.[45,46] In addition to cuproptosis, we also found that pyroptosis was depressed in ccRCC and that a pyroptosis-activated phenotype was associated with better clinical outcomes and a hot immune microenvironment.[55] Studies from previous works also revealed that inducing PCD inducing necroptosis, pyroptosis and autophagy could stimulate the release of cancer antigens, thus priming immune cell infiltration and promoting the maturation of tertiary lymphoid structures.[56] All these findings suggest that PCD is out of control in cancer tissues and that restoring the normal state of PCD levels could enhance other forms of cancer therapies, including targeted and immune-related agents.

Prior research has investigated the molecular and clinical attributes of different types of cell death in tumors, with a particular focus on disulfidptosis in both oncological and non-oncological conditions at various omics levels.[57,58] For example, Huang et al. developed a new prognostic model based on disulfidptosis in lung adenocarcinoma, revealing associations with the tumor microenvironment. Patients classified into the high-risk category displayed elevated tumor purity and decreased stromal score, ESTIMATE score, and Immune score.[59] Chen et al. conducted a thorough investigation into disulfidptosis in bladder cancer (BCa), elucidating its role in the modulation of tumor advancement, response to treatment, and overall survival among BCa patients. Additionally, the study identified POU5F1 and CTSE as promising targets for potential therapeutic interventions in the clinical management of BCa.[60] A study conducted by Xie et al. demonstrated a correlation between disulfidptosis activity and key biological processes and pathways in different types of cancers. This activity was found to be linked to tumor immune characteristics and predictive of immunotherapy outcomes. Specifically, the regulator of disulfidptosis, GYS1, was identified as a potential target for triple-negative breast cancer and validated through both *in vitro* and *in vivo* experiments.[61] These findings offer valuable insights into cancer progression and potential strategies for precise management. Until now, there has been no comprehensive analysis of disulfidptosis in ccRCC, and the potential interaction between disulfidptosis and the tumor microenvironment is largely unclear. In this work, we first conducted a pancancer analysis of ten disulfidptosis hits and found a uniform phenomenon in which nearly all disulfidptosis hits and scores were downregulated in cancers. In detail, such aberrant expression patterns might be caused by abnormal methylation and mutation events, which are obvious in uterine corpus endometrial carcinoma, skin cutaneous melanoma, and colon adenocarcinoma. In ccRCC patients, we performed a cluster analysis and deciphered four subtypes with distinctive biological and prognostic characteristics, and the results were reproduced in two independent datasets. Importantly, we found several candidate agents that are officious for DCS3 and verified these findings in corresponding subtype-specific cell lines, which could inhibit cell proliferation and metastasis. The role of SLC7A11 was also investigated at multiple levels and displayed an oncogenic role in ccRCC. Furthermore, these four distinct phenotypes exhibited notable differences in their molecular alteration landscape and activation of signaling pathways, resulting in varying metabolic processes and biological behaviours (Supplementary Table 5).

Similar to other tumors, the heterogeneity of ccRCC prognosis stems from intrinsic molecular alterations. Currently, the development of high-throughput sequencing and bioinformatics promotes the elucidation of comprehensive molecular alteration landscape in ccRCC. Many novel molecular clustering systems were established based on different altered molecules and forms. For instance, Hu et al. identified a novel ccRCC subtype, termed as De-clear cell differentiated (DCCD)-ccRCC, via multi omics datasets including genomic, transcriptomic, proteomic, metabolomic and spatial transcriptomic and metabolomic profiles from Tongji Hospital RCC (TJ-RCC) cohort.[62] Their work revealed that ccRCC patients owing fewer lipid droplets, reduced metabolic activity, enhanced nutrient uptake capability and a high proliferation rate, led to a relatively poor prognosis. The RCC program of TRACERs categorized ccRCC into seven primary subtypes, which include VHL monodriver, PBRM1-SETD2, PBRM1 somatic copy number alteration (SCNA), PBRM1-PI3K, VHL wildtype, multiple clonal drivers, and BAP1 driven. These distinct genomic subtypes displayed a notably diverse prognosis.[63] Furthermore, Meng et al. conducted a consensus analysis of ccRCC utilizing multiple omics datasets.[64] Among these subtypes, MoS1 exhibited the worst prognosis, potentially due to an immunosuppressed microenvironment and activated hypoxia characteristics but may respond

positively to PI3K/AKT inhibitors. MoS2 displayed a higher frequency of mutations in VHL and PBRM1, indicating a more favourable prognosis and potential suitability for sunitinib therapy. MoS3 was identified as the immune hot subtype, suggesting potential benefits from anti-PD-1 immunotherapy. Undoubtedly, the subtyping studies mentioned above, through diverse gene sets or specific clustering algorithms, have identified particular subtypes of ccRCC patients, offering new insights for personalized treatment of ccRCC. Similarly, this study, by systematically analysing the clinical and biological roles of disulfidptosis signaling in pan-cancer and ccRCC, classifies ccRCC into four subtypes, among which the DCS3 subtype is associated with the worst prognosis and has been validated across multiple ccRCC cohorts. In this subtype, pathways related to keratinization and resistance to apoptosis are significantly activated. Ultimately, we discovered that NU1025 could act as a sensitive drug for the DCS3 subtype.

Studies have shown that the extensive immune infiltrative, highly vascularized, and fibrotic nature of the TME in ccRCC compared to other solid tumors not only supports the use of immunotherapy but also has a significant impact on patient response through its complex effects.[65,66] However, the interaction between cell death and the TME and whether disulfidocytosis can promote immune infiltration in ccRCC are unclear. We found that antitumour immunity was hampered in DCS3, even though the immune score calculated in the ESTIMATE algorithm was the highest among the four types. Such a paradox could be referred to as deficiency of DNA repair and tumor antigen presentation, which induced persistent production of ineffective genomic-derived antigens. Consistently, when comparing the genomic mutation landscape among the four types, we found that the copy number alteration rate was highest in DCS3, which resulted in a high TMB. In addition, DCS3 led the lowest response rate to ICI (only 26% compared with 42% in DCS4) and cytolytic activity (CYT) score. Interestingly, Liu found that patients with characteristics of TMB high and CNA low might reach an optimal therapy result to ICI.[67] The results were different with our findings in DCS4 and could be explained by accumulating CNA with deficient ability of repair inducing antigens of no tumor biological futures.[68] We found that keratin signaling was significantly activated in DCS3, which might help explain the complicated TME in this type. Indeed, several previous works have proven their roles in cancer progression and tumor immunity.[69] Research from Wang et al. suggested that tumor cells could release the coating structure of CXCL12-KRT19, thus mediating CD8 T-cell exclusion. Wang and colleagues found a classic keratin family member, K17, which was highly expressed in head and neck squamous cell carcinoma, and knockout of K17 could reverse ICI resistance in a T-cell-dependent manner.[70] The positive correlation of immune signature and keratins was also found in conjunctive melanoma.[71] All these findings suggest that keratin-related proteins participate in cancer immune evasion.

To maximize the potential benefits of immunotherapy, several clinical trials have combined anti-PD-1/PD-L1 antibodies with anti-CTLA-4 antibodies or TKIs as first-line treatment for ccRCC.[72] Some recently published results showed that combination therapy is overall better than TKI monotherapy.[73] Although combination therapy has become the first-line treatment option for mRCC, not all patients benefit from it, and serious side effects can occur.[74,75] For example, in the KEYNOTE-426 trial, the most common adverse events with the combination of axitinib and pembrolizumab were diarrhea and hypertension, and the incidence of liver toxicities was higher than with monotherapy, with 30.5% of patients having to discontinue at least one treatment due to adverse events.[72] We hypothesized that reactivating disulfidocytosis in ccRCC could enhance immune therapeutic efficacy in ccRCC. Interestingly, we found that NU1025, a potent PARP inhibitor, might be useful for DCS3. When culturing ccRCC cell lines with the addition of NU1025, the malignant biological behaviours of ccRCC were significantly hampered, which preliminarily suggested that NU1025 could be utilized as a novel agent for ccRCC therapy. Basically, NU1025 does not affect cell viability at normal concentrations and only works in specific cancer cell lines, including BRCA mutation breast cancer.[76] Koustas found that the combination of the coinhibition effect of SU11274 (a c-MET inhibitor) and NU1025 could reduce tumor proliferation and trigger PCD in gastric cancer.[77] Taken together, these results suggest that NU1025 functions as a novel weapon for ccRCC patients with high risk and deficiency in disulfidptosis signaling.

It is worth noting that one of the notorious characteristics of ccRCC is activated glucose intake and consumption, followed by aberrant metabolic reprogramming. Previous works found that SLC7A11 was involved in PCD in ccRCC via different signals. Xu et al. revealed that SLC7A11 involve in ccRCC prognosis and promoted by inhibiting ferroptosis.[78] SLC7A11 is also involved in ferroptosis depression as a downstream factor of the MITD1-TAZ and PDIA1-ATF4 pathways in ccRCC.[79] We also found that SLC7A11 acted as the most important variable among ten disulfidptosis hits, and the prognostic impact was consistent across different ccRCC cohorts. We detected that the SLC7A11 expression level was higher in plasma and pDC cells at the single-cell level. Further studies should focus on investigating the immune impact of SLC7A11 in ccRCC.

Our work is the first comprehensive analysis of disulfidptosis across cancers and a detailed description of ccRCC, which shed new light on cancer diagnostics and management. Firstly, the disulfidptosis-related genes included in this study were limited to the top 10 genes identified by Liu et al. using the CRISPR-Cas9 technology. This gene set might only partially represent the activation or inhibition states of intracellular disulfidptosis, necessitating further basic research to fully elucidate the disulfidptosis signaling axis. Secondly, although potential therapeutic drugs for the DCS3 subtype, such as NU.1025, were preliminarily identified using the GDSC database and the NTP algorithm, and further validated through *in vitro* experiments, the efficacy of this agent, especially for patients with the DCS3 subtype, still requires additional molecular experiments, particularly *in vivo* studies, such as patient-derived xenografts or organoid models. Finally, the cohorts used in this study were all retrospective, and whether this molecular subtyping can accurately stratify renal cancer patients in real-world cohorts with precision risk stratification remains to be validated through the establishment of prospective cohorts.

5. Conclusions

In conclusion, our work investigated the role of disulfidptosis across cancers, especially in ccRCC. Four novel ccRCC subtypes were first identified with complicated biological and immune characteristics. Among these, DCS3, a subtype with inferior clinical outcomes, was suggested to be stratified from ccRCC patients with radical treatments. In *in vitro* experiments, we verified the therapeutic efficacy of NU1025 on DCS3-related cell lines and showed satisfactory therapeutic value. To conclude, this work provides novel insights into PCD and ccRCC, and we believe that disulfidptosis could help improve diagnosis and therapy for patients with ccRCC.

Declaration of competing interest

The authors declare that they have no known competing financial interests or personal relationships that could have appeared to influence the work reported in this paper.

Ethics statement

The cancer patient cohorts used in this work were publicly available datasets that were collected with patients' informed consent.

Availability of data and materials

All datasets and materials analysed in this work are summarized in the Methods section and are valuable under reasonable quest. The

code and data of this study is available in Github (https://github.com/jaingaimin/DCS_ccRCC).

Acknowledgements

All authors would like to thank Dr. Jianming Zeng from the University of Macau and his team Biotrainee for generously sharing their analysis experience. We would also like to thank Sangerbox for sharing their experience in visualization. This work was supported by the National Natural Science Foundation of China (grant numbers: 81902560, 81730073).

Author contributions

A.J., W.L., Y.L., J.H. and B.Z. performed formal analysis and experiments and contributed equally to this work. L.Q., C.C., P.L. and L.W. conceptualized and designed this study. Y.F., X.Z., B.Z., L.Q., J.L. and B.L. wrote and polished the draft. L.Q., P.L. and L.W. jointly conceived and supervised the study. All authors contributed to the article and approved the submitted version.

Supplementary materials

Supplementary material associated with this article can be found, in the online version, at doi:10.1016/j.jncc.2024.06.003.

References

1. Siegel RL, Miller KD, Fuchs HE, Jemal A. Cancer statistics, 2022. *CA Cancer J Clin*. 2022;72(1):7–33.
2. Siegel RL, Giaquinto AN, Jemal A. Cancer statistics, 2024. *CA Cancer J Clin*. 2024;74(1):12–49.
3. Ljungberg B, Albiges L, Abu-Ghanem Y, et al. European association of urology guidelines on renal cell carcinoma: the 2022 update. *Eur Urol*. 2022;82(4):399–410.
4. Xia C, Dong X, Li H, et al. Cancer statistics in China and United States, 2022: profiles, trends, and determinants. *Chin Med J*. 2022;135(5):584–590.
5. Han B, Zheng R, Zeng H, et al. Cancer incidence and mortality in China, 2022 Cancer incidence and mortality in China, 2022. *J Natl Cancer Cent*. 2024;4(1):47–53.
6. Wei H, Miao J, Cui J, et al. The prognosis and clinicopathological features of different distant metastases patterns in renal cell carcinoma: analysis based on the SEER database. *Sci Rep*. 2021;11(1):17822.
7. Mason RJ, Wood L, Kapoor A, et al. Kidney Cancer Research Network of Canada (KCRNC) consensus statement on the role of cytoreductive nephrectomy for patients with metastatic renal cell carcinoma. *Can Urol Assoc J*. 2019;13(6):166–174.
8. Tung I, Sahu A. Immune checkpoint inhibitor in first-line treatment of metastatic renal cell carcinoma: a review of current evidence and future directions. *Front Oncol*. 2021;11:707214.
9. Wahida A, Buschhorn L, Fröhling S, et al. The coming decade in precision oncology: six riddles. *Nat Rev Cancer*. 2023;23(1):43–54.
10. Xu W, Atkins MB, McDermott DF. Checkpoint inhibitor immunotherapy in kidney cancer. *Nat Rev Urol*. 2020;17(3):137–150.
11. Sharma R, Kadife E, Myers M, Kannourakis G, Prithviraj P, Ahmed N. Determinants of resistance to VEGF-TKI and immune checkpoint inhibitors in metastatic renal cell carcinoma. *J Exp Clin Cancer Res*. 2021;40(1):186.
12. Simonaggio A, Epaillard N, Pobel C, Moreira M, Oudard S, Vano YA. Tumor microenvironment features as predictive biomarkers of response to Immune Checkpoint Inhibitors (ICI) in Metastatic Clear Cell Renal Cell Carcinoma (mccRCC). *Cancers*. 2021;13(2):E231.
13. Linehan WM, Schmidt LS, Crooks DR, et al. The metabolic basis of kidney cancer. *Cancer Discov*. 2019;9(8):1006–1021.
14. Tong X, Tang R, Xiao M, et al. Targeting cell death pathways for cancer therapy: recent developments in necroptosis, pyroptosis, ferroptosis, and cuproptosis research. *J Hematol Oncol*. 2022;15(1):174.
15. Tsvetkov P, Coy S, Petrova B, et al. Copper induces cell death by targeting lipoylated TCA cycle proteins. *Science*. 2022;375(6586):1254–1261.
16. Li K, Tan L, Li Y, et al. Cuproptosis identifies respiratory subtype of renal cancer that confers favorable prognosis. *Apoptosis*. 2022;27(11–12):1004–1014.
17. Wang T, Liu Y, Li Q, Luo Y, Liu D, Li B. Cuproptosis-related gene FDX1 expression correlates with the prognosis and tumor immune microenvironment in clear cell renal cell carcinoma. *Front Immunol*. 2022;13:999823.
18. Liu X, Nie L, Zhang Y, et al. Actin cytoskeleton vulnerability to disulfide stress mediates disulfidptosis. *Nat Cell Biol*. 2023;25(3):404–414.
19. Colaprico A, Silva TC, Olsen C, et al. TCGAbiolinks: an R/Bioconductor package for integrative analysis of TCGA data. *Nucleic Acids Res*. 2016;44(8):e71.
20. Motzer RJ, Banchereau R, Hamidi H, et al. Molecular subsets in renal cancer determine outcome to checkpoint and angiogenesis blockade. *Cancer Cell*. 2020;38(6):803-17.e4.
21. Qu Y, Feng J, Wu X, et al. A proteogenomic analysis of clear cell renal cell carcinoma in a Chinese population. *Nat Commun*. 2022;13(1):2052.
22. Vasaikar SV, Straub P, Wang J, Zhang B. LinkedOmics: analyzing multi-omics data within and across 32 cancer types. *Nucleic Acids Res*. 2018;46(D1):D956–DD63.
23. Li Y, Dou Y, Da Veiga Leprevost F, et al. Proteogenomic data and resources for pan–cancer analysis. *Cancer Cell*. 2023;41(8):1397–1406.
24. Wilkerson MD, Hayes DN. ConsensusClusterPlus: a class discovery tool with confidence assessments and item tracking. *Bioinformatics*. 2010;26(12):1572–1573.
25. Love MI, Huber W, Anders S. Moderated estimation of fold change and dispersion for RNA-seq data with DESeq2. *Genome Biol*. 2014;15(12):550.
26. Liberzon A, Subramanian A, Pinchback R, Thorvaldsdóttir H, Tamayo P, Mesirov JP. Molecular signatures database (MSigDB) 3.0. *Bioinformatics*. 2011;27(12):1739–1740.
27. Yu G, Wang LG, Han Y, He QY. clusterProfiler: an R package for comparing biological themes among gene clusters. *OMICS*. 2012;16(5):284–287.
28. Lu X, Meng J, Zhou Y, Jiang L, Yan F. MOVICS: an R package for multi-omics integration and visualization in cancer subtyping. *Bioinformatics*. 2021;36(22–23):5539–5541.
29. Castro MAA, de Santiago I, Campbell TM, et al. Regulators of genetic risk of breast cancer identified by integrative network analysis. *Nat Genet*. 2016;48(1):12–21.
30. Fletcher MNC, Castro MAA, Wang X, et al. Master regulators of FGFR2 signalling and breast cancer risk. *Nat Commun*. 2013;4:2464.
31. Hänzelmann S, Castelo R, Guinney J. GSVA: gene set variation analysis for microarray and RNA-seq data. *BMC Bioinformatics*. 2013;14:7.
32. Xu L, Deng C, Pang B, et al. TIP: a web server for resolving tumor immunophenotype profiling. *Cancer Res*. 2018;78(23):6575–6580.
33. Yoshihara K, Shahmoradgoli M, Martínez E, et al. Inferring tumour purity and stromal and immune cell admixture from expression data. *Nat Commun*. 2013;4(1):2612.
34. Subramanian M, Kabir AU, Barisas D, Krchma K, Choi K. Conserved angio-immune subtypes of the tumor microenvironment predict response to immune checkpoint blockade therapy. *Cell Rep Med*. 2023;4(1):100896.
35. Mayakonda A, Lin DC, Assenov Y, Plass C, Koeffler HP. Maftools: efficient and comprehensive analysis of somatic variants in cancer. *Genome Res*. 2018;28(11):1747–1756.
36. Mermel CH, Schumacher SE, Hill B, Meyerson ML, Beroukhim R, Getz G. GISTIC2.0 facilitates sensitive and confident localization of the targets of focal somatic copy-number alteration in human cancers. *Genome Biol*. 2011;12(4):R41.
37. Cokelaer T, Chen E, Iorio F, et al. GDSCTools for mining pharmacogenomic interactions in cancer. *Bioinformatics*. 2018;34(7):1226–1228.
38. Geeleher P, Cox N, Huang RS. pRRophetic: an R package for prediction of clinical chemotherapeutic response from tumor gene expression levels. *PLoS One*. 2014;9(9):e107468.
39. Qu L, Wu Z, Li Y, et al. A feed-forward loop between lncARSR and YAP activity promotes expansion of renal tumour-initiating cells. *Nat Commun*. 2016;7:12692.
40. Gu D, Dong K, Jiang A, et al. PBRM1 deficiency sensitizes renal cancer cells to DNMT inhibitor 5-fluoro-2'-deoxycytidine. *Front Oncol*. 2022;12:870229.
41. Gong H, Jiang A, Jiang R, et al. PTBP1 as a promising predictor of poor prognosis by regulating cell proliferation, immunosuppression, and drug sensitivity in SARC. *Oxid Med Cell Longev*. 2022;2022:5687238.
42. Zeng D, Ye Z, Shen R, et al. IOBR: multi-omics immuno-oncology biological research to decode tumor microenvironment and signatures. *Front Immunol*. . 2021;12:687975.
43. Liu CJ, Hu FF, Xie GY, et al. GSCA: an integrated platform for gene set cancer analysis at genomic, pharmacogenomic and immunogenomic levels. *Brief Bioinform*. 2023;24(1):bbac558.
44. Liu CJ, Hu FF, Xia MX, Han L, Zhang Q, Guo AY. GSCALite: a web server for gene set cancer analysis. *Bioinformatics*. 2018;34(21):3771–3772.
45. Jiang A, Luo P, Chen M, et al. A new thinking: deciphering the aberrance and clinical implication of copper-death signatures in clear cell renal cell carcinoma. *Cell Biosci*. 2022;12(1):209.
46. Jiang A, Ye J, Zhou Y, et al. Copper death inducer, FDX1, as a prognostic biomarker reshaping tumor immunity in clear cell renal cell carcinoma. *Cells*. 2023;12(3):349.
47. Jiang A, Liu Y, Zhu B, et al. SPCS, a novel classifier system based on senescence axis regulators reveals tumor microenvironment heterogeneity and guides frontline therapy for clear cell renal carcinoma. *Clin Genitourin Cancer*. 2024;22(2):497–513.
48. Jiang A, Xu Z, Fang X, et al. RNA modification pattern-based subtypes reveal heterogenous clinical outcomes and tumor immunity of clear cell renal cell carcinoma. *MedComm*. 2023;2(1):e30.
49. Yi F, Frazzette N, Cruz AC, Klebanoff CA, Siegel RM. Beyond cell death: new functions for TNF family cytokines in autoimmunity and tumor immunotherapy. *Trends Mol Med*. 2018;24(7):642–653.
50. Broz P, Pelegrín P, Shao F. The gasdermins, a protein family executing cell death and inflammation. *Nat Rev Immunol*. 2020;20(3):143–157.
51. Erkes DA, Cai W, Sanchez IM, et al. Mutant BRAF and MEK inhibitors regulate the tumor immune microenvironment via pyroptosis. *Cancer Discov*. 2020;10(2):254–269.
52. Rosenbaum SR, Wilski NA, Aplin AE. Fueling the fire: inflammatory forms of cell death and implications for cancer immunotherapy. *Cancer Discov*. 2021;11(2):266–281.
53. Braun DA, Street K, Burke KP, et al. Progressive immune dysfunction with advancing disease stage in renal cell carcinoma. *Cancer Cell*. 2021;39(5):632–648.e8.
54. Demuynck R, Efimova I, Naessens F, Krysko DV. Immunogenic ferroptosis and where to find it? *J Immunother Cancer*. 2021;9(12):e003430.
55. Jiang A, Meng J, Bao Y, et al. Establishment of a prognosis prediction model based on pyroptosis-related signatures associated with the immune microenvironment and molecular heterogeneity in clear cell renal cell carcinoma. *Front Oncol*. . 2021;11:4486.
56. Chen L, Min J, Wang F. Copper homeostasis and cuproptosis in health and disease. *Signal Transduct Target Ther*. 2022;7(1):378.
57. Mao C, Wang M, Zhuang L, Gan B. Metabolic cell death in cancer: ferroptosis, cuproptosis, disulfidptosis, and beyond. *Protein Cell*. 2024:pwae003.

58. Liu Z, Zhao Q, Zuo ZX, et al. Systematic analysis of the aberrances and functional implications of ferroptosis in cancer. *iScience*. 2020;23(7):101302.
59. Luo Y, Liu L, Zhang C. Identification and analysis of diverse cell death patterns in diabetic kidney disease using microarray-based transcriptome profiling and single-nucleus RNA sequencing. *Comput Biol Med*. 2024;169:107780.
60. Chen H, Yang W, Li Y, Ma L, Ji Z. Leveraging a disulfidptosis-based signature to improve the survival and drug sensitivity of bladder cancer patients. *Front Immunol*. 2023;14:1198878.
61. Xie J, Deng X, Xie Y, et al. Multi-omics analysis of disulfidptosis regulators and therapeutic potential reveals glycogen synthase 1 as a disulfidptosis triggering target for triple-negative breast cancer. *MedComm*. 2024;5(3):e502.
62. Hu J, Wang SG, Hou Y, et al. Multi-omic profiling of clear cell renal cell carcinoma identifies metabolic reprogramming associated with disease progression. *Nat Genet*. 2024;56(3):442–457.
63. Turajlic S, Xu H, Litchfield K, et al. Deterministic evolutionary trajectories influence primary tumor growth: TRACERx renal. *Cell*. 2018;173(3):595–610.e11.
64. Meng J, Jiang A, Lu X, et al. Multiomics characterization and verification of clear cell renal cell carcinoma molecular subtypes to guide precise chemotherapy and immunotherapy. *iMeta*. 2023;2:e14.
65. Geissler K, Fornara P, Lautenschläger C, Holzhausen HJ, Seliger B, Riemann D. Immune signature of tumor infiltrating immune cells in renal cancer. *Oncoimmunology*. 2015;4(1):e985082.
66. Sato Y, Yoshizato T, Shiraishi Y, et al. Integrated molecular analysis of clear-cell renal cell carcinoma. *Nat Genet*. 2013;45(8):860–867.
67. Liu L, Bai X, Wang J, et al. Combination of TMB and CNA stratifies prognostic and predictive responses to immunotherapy across metastatic cancer. *Clin Cancer Res*. 2019;25(24):7413–7423.
68. Samstein RM, Lee CH, Shoushtari AN, et al. Tumor mutational load predicts survival after immunotherapy across multiple cancer types. *Nat Genet*. 2019;51(2):202–206.
69. Ogunnigbagbe O, Bunick CG, Kaur K. Keratin 1 as a cell-surface receptor in cancer. *Biochim Biophys Acta Rev Cancer*. 2022;1877(1):188664.
70. Wang Z, Moresco P, Yan R, et al. Carcinomas assemble a filamentous CXCL12-keratin-19 coating that suppresses T cell-mediated immune attack. *Proc Natl Acad Sci USA*. 2022;119(4):e2119463119.
71. Cisarova K, Folcher M, El Zaoui I, et al. Genomic and transcriptomic landscape of conjunctival melanoma. *PLoS Genet*. 2020;16(12):e1009201.
72. Rini BI, Plimack ER, Stus V, et al. Pembrolizumab plus axitinib versus sunitinib for advanced renal-cell carcinoma. *N Engl J Med*. 2019;380(12):1116–1127.
73. Motzer RJ, Tannir NM, McDermott DF, et al. Nivolumab plus Ipilimumab versus Sunitinib in advanced renal-cell carcinoma. *N Engl J Med*. 2018;378(14):1277–1290.
74. Lombardi P, Filetti M, Falcone R, et al. New first-line immunotherapy-based combinations for metastatic renal cell carcinoma: a systematic review and network meta–analysis. *Cancer Treat Rev*. 2022;106:102377.
75. Hofmann F, Hwang EC, Lam TB, et al. Targeted therapy for metastatic renal cell carcinoma. *Cochrane Database Syst Rev*. 2020;10(10):CD012796.
76. Węsierska-Gądek J, Mauritz M, Mitulovic G, Cupo M. Differential potential of pharmacological PARP inhibitors for inhibiting cell proliferation and inducing apoptosis in human breast cancer cells. *J Cell Biochem*. 2015;116(12):2824–2839.
77. Koustas E, Karamouzis MV, Sarantis P, Schizas D, Papavassiliou AG. Inhibition of c-MET increases the antitumour activity of PARP inhibitors in gastric cancer models. *J Cell Mol Med*. 2020;24(18):10420–10431.
78. Xu F, Guan Y, Xue L, et al. The roles of ferroptosis regulatory gene SLC7A11 in renal cell carcinoma: a multi-omics study. *Cancer Med*. 2021;10(24):9078–9096.
79. Kang L, Wang D, Shen T, et al. PDIA4 confers resistance to ferroptosis via induction of ATF4/SLC7A11 in renal cell carcinoma. *Cell Death Dis*. 2023;14(3):193.